Journal of Ultrafine Grained and Nanostructured Materials
https://jufgnsm.ut.ac.ir
Vol. 53, No.1, June 2020, pp. 23-30
Print ISSN: 2423-6845 Online ISSN: 2423-6837
DOI: 10.22059/jufgnsm.2020.01.04

Effect of calcination process on the gas phase photodegradation by CuO-Cu_2O/TiO_2 nanocomposite photocatalyst

Fahimeh Ansari[1], Saeed Sheibani*[*,1], Uriel Caudillo-Flores[2], Marcos Fernández-García[2]

[1]School of Metallurgy and Materials Engineering, College of Engineering, University of Tehran, Tehran, Iran.
[2]Instituto de Catálisis y Petroleoquímica, CSIC. C/ Marie Curie, 2, 28049, Madrid, Spain.

Recieved: 1 June 2020; Accepted: 20 June 2020
** Corresponding author email: ssheibani@ut.ac.ir*

ABSTRACT

A series of CuO-Cu_2O/TiO_2 nanocomposite samples were prepared by the sol-gel method. Before applying the sol-gel method, the $Cu(OH)_2$ nanostructure on Cu powders were formed by in-situ solution treatment. The samples were characterized through some techniques and the photocatalytic performance of CuO-Cu_2O/TiO_2 nanocomposites for gas-phase 2-propanol photo-oxidation under UV and sunlight type illumination was evaluated. The effect of calcination process on the synthesis and photocatalytic activity of the samples was studied. The calcination process plays an important role in improving the properties of nanocomposite powders. The results showed that the nanocomposite formed successfully in desirable structure and morphology. The nanocomposite is composed by the mixture of TiO_2 particle with an average particle size of about 300 nm and the copper oxide nanorods with a diameter of 50-100 nm. In this nanocomposite, the copper oxides nanostructures and TiO_2 particles are the main components to form the heterojunction structure and provide enhanced photocatalytic performance compared to the TiO_2 sample. The reaction rate of the most active nanocomposite sample prepared at the optimum conditions is almost 6 times larger than the TiO_2 references.

Keywords: *Copper Oxide; TiO_2; Nanocomposite; Gas Phase Photodegradation; Calcination.*

1. Introduction

Recently, heterogeneous photocatalysis with using semiconductors has been well accepted as a modern technology used in gas or liquid chemical reactions for the elimination of organic and inorganic pollutants [1,2]. Among various semiconductor photocatalysts, cupric oxide (CuO) and cuprous oxide (Cu_2O) have been considered as promising materials for photocatalytic applications because of their beneficial advantages [3,4]. Copper oxide photocatalysts display strong light absorption ability and effective narrow band gap energy (E_{bg}) positions of 1.2-1.7 eV and 2.0-2.2 eV for CuO and Cu_2O, respectively [3,5]. Moreover, excellent environmental accessibility, non-toxicity, earth abundant and low cost are the other properties of copper oxides [4]. However, instability in reaction conditions because of photocorrosion under light illumination is the disadvantage of copper oxide materials [6,7]. Researchers have stated that fabrication the heterogeneous semiconductors with combining photocatalysts is a beneficial approach to overcome the shortages of copper oxide materials [7,8]. The n-type TiO_2 has been recognized as the most important photocatalyst because of chemical stability, non-toxicity, and low costs. However, high band gap energy (3.0-3.2 eV) and the rapid recombination of photoinduced

electron-hole pairs of TiO_2 has been remarkably limited its photocatalytic performance [9]. Hence, control of the recombination of photogenerated charge carriers of TiO_2 as well as stabilizing the copper oxide components improvement of the visible light photocatalytic performance are essential for photocatalytic applications. As is well reported, combining TiO_2 with narrow band gap semiconductors has attracted attention to improve its visible-light photocatalytic properties as well as to overcome drawbacks of the components [7,10]. Researches have proved that the preparation of heterojunction structure with TiO_2 and copper oxides leads to an enhancement of the photocatalytic performance of the composite [11,12]. CuO-Cu_2O/TiO_2 heterojunction nanocomposite can promote the photocatalytic performance through photoinduced pairs of electron-hole separation and increase of the charge carriers lifetime. Furthermore, the generation of heterostructure combining TiO_2 nanoparticles and copper oxide components will solve photocorrosion problem and improve the stability of the nanocomposite structures [7,13]. On other hand, 2-propanol (IPA) is a typical volatile organic pollutant present in the urban atmospheres and especially at indoor environments. The construction materials, household products, waxes, varnishes, and many others are the typical sources of this pollutant. The elimination of 2-propanol is necessary for the environment protection and human health. Furthermore, its photo-oxidation has been used as a model for photocatalyst materials [14].

The main aim of the present work is design and synthesize a novel CuO-Cu_2O/TiO_2 nanocomposites with desirable morphology and properties to enhance the photocatalytic performance. In this contribution, the CuO-Cu_2O nanostructures on pure Cu powders were fabricated by in-situ solution treatment - thermal oxidation and consequently decorate the TiO_2 nanoparticles on the surface. The nanoparticles decorating was accomplished by the hydrolyzation process followed by a calcination treatment to stabilize them as well as enhance their activity. In this study, the thermal oxidation and calcination process have been merged. The samples were characterized through the techniques including X-ray diffraction (XRD), inductively coupled plasma atomic emission spectroscopy (ICP-AES), Brunauer-Emmett-Teller (BET) method, Field Emission Scanning Electron Microscopy (FESEM) and UV-vis spectroscopy. The gas-phase 2-propanol photo-oxidation was employed for photocatalytic performance of CuO-Cu_2O/TiO_2 composites under UV and sunlight type illumination by computing the reaction rate. By comparison, the effect of calcination process on the photo-oxidation performance and stability of nanocomposites was investigated.

2. Materials and methods

2.1. Preparation and characterization of the samples

Copper powder (99%, particle size <45 micron), sodium hydroxide (NaOH) and persulfate ammonium ($(NH_4)_2S_2O_8$) were used for formation of as-synthesized $Cu(OH)_2$ nanorods. Tetrabutyl-orthotitanate (TBOT, $C_{16}H_{38}O_4Ti$) as a titanium precursor, ethanol (EtOH, C_2H_5OH) as a solvent, deionized water for hydrolysis, (BA, C_7H_8O) as a surfactant were employed in the sol-gel process. The CuO-Cu_2O nanostructures on Cu surface have been synthesized via the in-situ chemical oxidation with further thermal treatment that merged with the calcination step in sol-gel method. The thermal transformation of $Cu(OH)_2$ nanorods templates, which were fabricated through a chemical oxidation process lead to the fabrication of the CuO-Cu_2O nanostructures. First, a mixed aqueous solution of 25 ml of 2.5 M NaOH and 25 ml 0.2 M $(NH_4)_2S_2O_8$ was prepared and then the high purity Cu powders were immersed in the solution. After 30 minutes, a blue color appeared in the initially colorless solution and the Cu powders were extracted from the solution, thoroughly were rinsed with distilled water, and were dried in air. In this stage, the $Cu(OH)_2$ on Cu powders were synthesized. Then, TiO_2 particles were formed on the surface of the pre-treated powders to form the $Cu(OH)_2$ nanostructures by the sol-gel process. The obtained pre-treated powders were dispersed in hydrolysis solution prepared with the mixing of EtOH, BA and distilled water at room temperature. Then, the 0.5 M TBOT solution was added slowly drop by drop into the hydrolysis solution under vigorous stirring and stirred for three hours. The reaction was carried out using TBOT:BA:EtOH:H_2O molar ratio of 1:5:100:5. Finally, the resulting sample dried in air at room temperature for 24 hours and heat treated at two diffrent calcination process. The heating rate was maintained at 5°C/min in all the thermal oxidation experiments, and after that, samples were taken out the furnace for characterization. The influence of heat treatment type and temperature

on morphology, structure and photocatalytic properties were investigated. The calcination processes were chosen at two temperatures of 400 and 500°C under air atmosphere. Samples are labeled T for TiO_2 reference and C1 and C2 for nanocomposite samples. The heat treatment for C1 sample was carried out at temperature of 400°C for 1 h as the one-step process. For C2 nanocomposite sample, the temperature was first raised to 300°C and maintained for 30 min. Then, the samples were heated to 500°C and maintained for another 30 min.

The crystal structure and composition of the samples were analyzed via XRD analysis. The recording X-ray diffraction data was carried out from 2θ of 10 to 90° on a Seifert D-500 diffractometer using Ni-filtered Cu K_α radiation (λ=0.15406 nm) with a 0.02° step. Rietveld analysis was performed by using Xpert High Score Plus software for samples. ICP-AES using a Perkin-Elmer Optima 3300 DV spectrometer was used for the elemental analysis of the nanocomposite samples. The samples for BET analysis were degassed under flowing argon at 473K for 2 h before nitrogen adsorption. FESEM images were obtained using a CamScan MV2300 scanning electron microscope for morphological evaluation. The particle size determination from FESEM results was accomplished via Image-J software. UV-vis diffuse-reflectance spectroscopy (DRS) experiments were done on a Shimadzu UV2100 apparatus using $BaSO_4$ as a reference that does not absorb in the UV-vis radiation range. The results were recorded in the diffuse reflectance mode (R). The Kubelka-Munk function F(R) was applied for the conversion of the spectra obtained from UV-vis measurements [8,15].

2.2. Photocatalytic performance

The activity of the photocatalysts was tested using a continuous flow annular photo-reactor (Pyrex tube). A certain amount of catalyst (ca. 2 mg cm^{-2}) was prepared as a suspension in methanol, painted as a thin layer on the inner tube (cut-off at ca. 290 nm) and dried at room temperature. The irradiation was generated by four fluorescent lamps (UV: 6W; Sylvania F6WBLT-65; Sunlight-type: 6W, Sylvania F6W/D) symmetrically put outside the reactor. Pure N_2 and O_2 were utilized for preparing the reacting mixture (100 mL min^{-1} and 20 vol% O_2/N_2). Carrying the gas-phase products from the liquid-containing saturator to the mainstream by N_2/O_2 mixture. To achieve a relative humidity at the gas flow, distilled water was injected by a syringe pump. To determine the concentration of the reactant and products of the photooxidation reactions, an online gas chromatograph instrument (Agilent GC 6890) equipped with HP-PLOT-Q/ HP-Innowax columns (0.5/0.32mm I.D. × 30 m) and thermal conductivity and flame ionization detectors (TCD/FID) was employed. A thermal conductivity detector was used to measure the CO_2 production and flame ionization detector was utilized to detect the 2-propanol and acetone as the organic components in the reaction. The photocatalytic behavior of the samples for gas-phase 2-propanol photodegradation was evaluated using reaction rate measurements and selectivity of the products. Reaction rates were obtained under steady state conditions, achieved usually after 4-5 h from the start of irradiation. The reaction rate normalized by catalytic area according to the Equation (1), where r is the reaction rate, C and C_0 are the concentration of 2-propanol at times t and t=0, Q is the total flow, S_A is the catalytic area and m is the mass used in the reaction.

$$\langle r \rangle = Q\left(\frac{\langle C_0 \rangle - \langle C \rangle}{m\ S_A}\right) \quad (1)$$

3. Results and discussion

XRD analysis was carried out to study the phase and crystal structure of the samples (Fig. 1). The XRD pattern of initial pure Cu powders (JCPDS Card No. 04-0836) is shown in Fig. 1(a) for comparison. After immersion the powders in the solution for pretreatment, small peaks of orthorhombic $Cu(OH)_2$ (JCPDS Card No. 80-0656) were observed in addition to the Cu peaks. However, the low intensity of diffraction peaks corresponding to $Cu(OH)_2$ in the XRD patterns was due to its small quantity on the surface of Cu powder. The XRD pattern of T sample (Fig. 1(c)) displays only the peaks associated with the anatase TiO_2. For the C1 and C2 samples, the peaks were obtained from the samples dominantly belong to Cu, CuO (JCPDS Card No. 48-1548) and Cu_2O (JCPDS Card No. 78-2076). It seems that the different calcination process conditions form mixed phases of copper species with different properties [16]. Probably, lower temperature of the calcination step of synthesis led to the formation of different copper species mostly with lower valence (Cu^0 and Cu^{+1}). Interestingly, a small peak of TiO_2 related to the anatase (101) located at 25.6° is observed (notice the enlarged view of the peaks at 2θ range

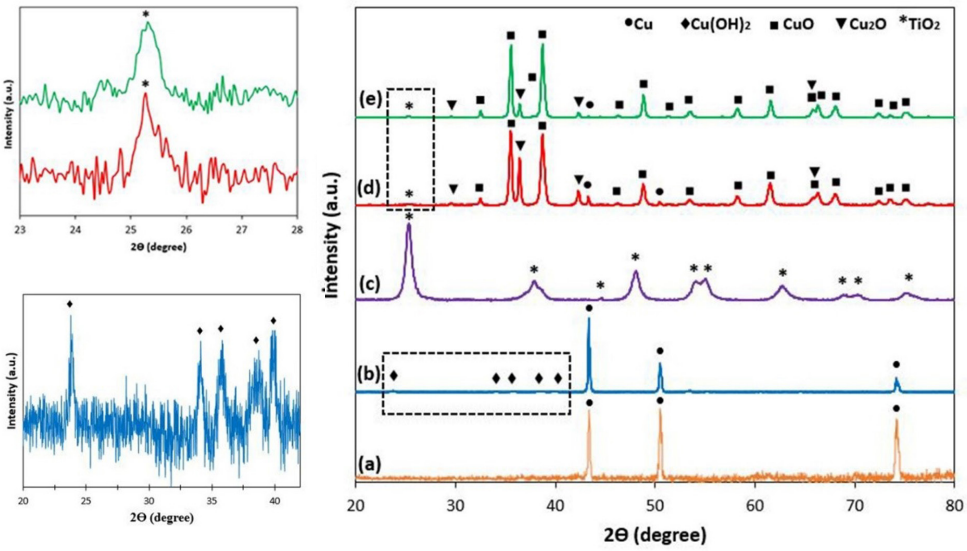

Fig. 1- XRD patterns of (a) pure copper powder, (b) as-synthesized Cu-$Cu(OH)_2$, (c) T, (d) C1 and (e) C2 samples.

Table 1- Ti/Cu ratio, BET surface area, pore volume and pore size values of studied samples

sample	Ti/Cu ratio	BET surface area (m^2g^{-1})	Pore volume (cm^3g^{-1})	Pore size (nm)
C1	0.027	3.11	0.016	13.71
C2	0.028	2.03	0.014	18.10

of 23 to 28° in the inset). It should be noted that the low intensity of diffraction peak corresponding to the TiO_2 phase in the XRD patterns of composite samples is related to its small quantity on the surface and XRD analysis limitations. On the other hand, the ICP-AES analysis results in Table 1 prove the existence of Ti and Cu elements in the composite samples. The calculated molar ratio between Ti and Cu in composite materials is approximately 0.03.

The surface area, pore volume and pore size results of the samples obtained from BET measurements are reported in Table 1. The results show that the samples are mesostructured materials (IUPAC definition: pore size 2-50 nm) [17]. Moreover, the higher surface area and decreased pore size is observed for C1 compared to C2 sample. As is reported, the surface area could play an important role in photocatalytic activities [18].

As illustrated in the FESEM micrographs in Fig. 2, the initial Cu powders have a relatively rough surface with no obvious indication of any other phases (Fig. 2(a)). As can be seen in Fig 2(b), the as-synthesized $Cu(OH)_2$ nanorod structures with a diameter of 50-100 nm smoothly and completely cover the copper sufrace after chemical oxidation step for solution treatment. The detailed study of $Cu(OH)_2$ formation on the Cu surface and then transformation to the copper oxides was performed in our previous work [19]. FESEM image of T sample after calcination in Fig. 2 (c) shows spherical TiO_2 nanoparticles with the average particle size of about 300 nm. The comparison of the FESEM image of composite sample before (Fig. 2(d)) and after calcination (Fig. 2(e and f)) reveals that the amorphous $Ti(OH)_4$ agglomerates generate selectively on the $Cu(OH)_2$ nanorod surfaces and during calcination process, the amorphous $Ti(OH)_4$ layer shrank to generate TiO_2 and formed the decorated nanoparticles on the surface [8,20]. The image for C1 sample after calcination shows that the surface is decorated by the mixture of TiO_2 nanoparticle and copper oxide nanorods. The detailed study of the machanism formation of copper oxide nanorods [19] and TiO_2 nanoparticles [20] is investigated in our previous works. As it is obvious in Fig. 2 (f), less nanorod morphology and decresed uniformity of nanospherical particles is observed compared to C1 sample. Apparantly, the nanorods were unstable probably due to the high-temperature reactions that cause in the missing the special morphology. Therefore, maybe applying lower temperature for calcination step is more

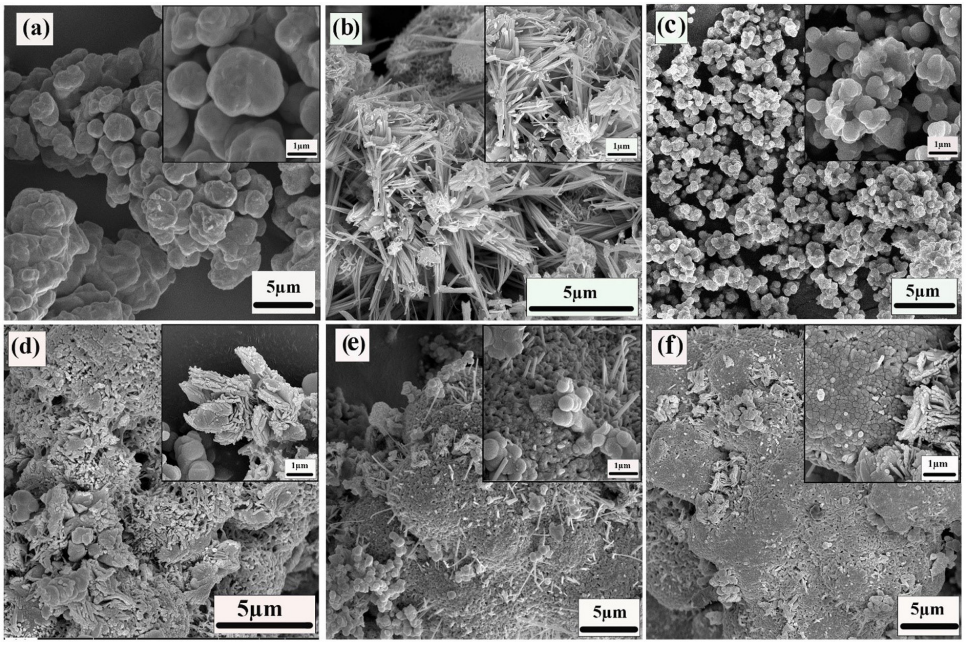

Fig. 2- FESEM images of (a) pure copper powder, (b) as-synthesized Cu-$Cu(OH)_2$, (c) T, (d) composite sample before calcination, (e) C1 and (f) C2.

appropriate to achieve the desirable morphology with higher surface which will be beneficial to the photocatalytic activity.

The optical properties of the prepared samples were evaluated in Fig. 3 in term of Kubelka-Munk equivalent absorbance units. The T sample indicated the characteristic spectrum with a sharp absorption band edge at ~400 nm in UV region, which corresponds to the anatase phase [10]. The nanocomposite samples demonstrated a much-enhanced light absorption in the visible light region, indicating the well-combination of semiconductors to achieve the heterojunction [13,21]. In this nanocomposite photocatalysts, copper oxides act as the main visible light absorber and titania formed heterojunction with the copper oxides which is useful for photocatalytic performance [8]. As can be seen, the nanocomposite materials display two dominant features. The nanocomposite catalysts demonstrate stopping edge at around 400 and 420 nm, which correspond to titania in the samples. Moreover, the feature located at around 850 nm in the UV-vis spectra of CuO-Cu_2O/TiO_2 catalysts is associated to the Cu d-d transitions ($2E_g \rightarrow 2T_{2g}$ interband transitions) of Cu^{2+} clusters present in the structure [7].

The photocatalytic activity of the samples for 2-propanol photodegradation under both UV and sunlight illumination in terms of reaction rate

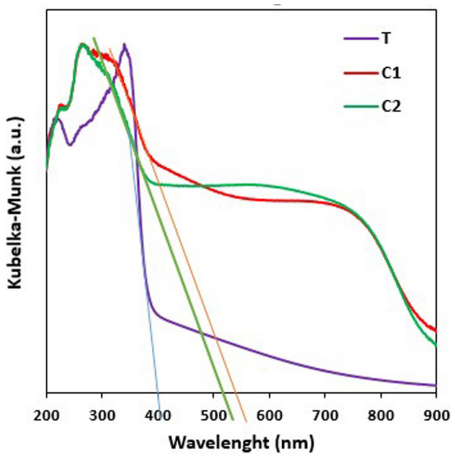

Fig. 3- UV-vis DRS spectra of different samples.

are depicted in Fig. 4. As it is obvious, the similar trends are observed in UV and sunlight-type illumination conditions. The calcination process conditions in the nanocomposite preparation play a significant role in the overall photocatalysis performance. Poor photocatalytic performance of T sample may be because of the wide band gap and rapid recombination of charge carriers [22]. The increased 2-propanol degradation is observed by formation the CuO-Cu_2O/TiO_2 nanocomposites especially for the C1 sample. The reaction rate of the most active nanocomposite sample is almost 6 times

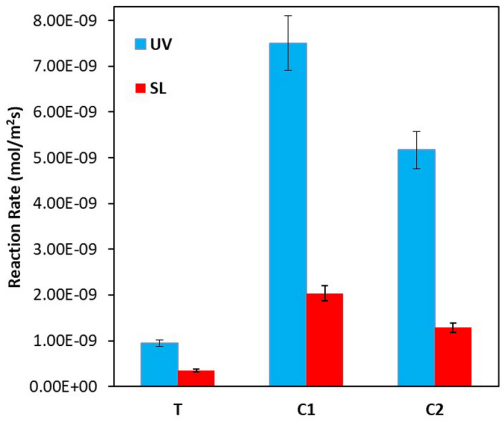

Fig. 4- 2-propanol photodegradation reaction rate under UV and solar light illumination for samples with different calcination process compared to the TiO_2 sample.

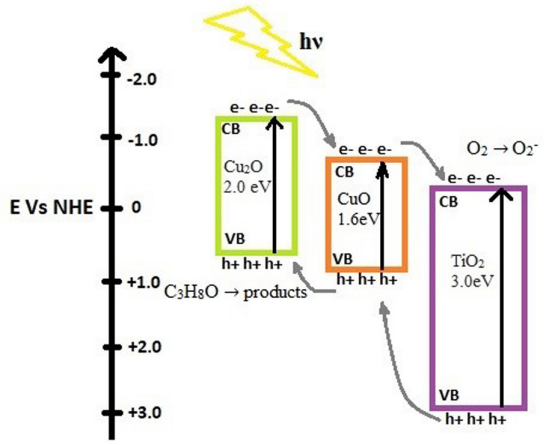

Fig. 5- Schematic illustration of the electronic band structures and proposed photodegradation mechanism of the heterojunction photocatalyst.

Table 2- Selectivity of the 2-propanol degradation under UV and sunlight illumination

Sample	Selectivity %(UV)		Selectivity %(SL)	
	CO_2	Acetone	CO_2	Acetone
T	59.40	40.60	84.20	15.80
C1	88.09	11.91	92.28	7.72
C2	88.87	11.13	90.39	9.61

larger than the TiO_2 references. This significant enhancement is possibly related to the presence of a mixture of various morphology of semiconductors with uniform distribution and relatively higher surface area. Moreover, the successful fabrication of the special heterostructure of CuO, Cu_2O and TiO_2 components could promote the activity of the nanocomposite [21,23]. The interface between CuO and Cu_2O act as a rapid separation site for photoinduced electron-hole pairs and consequently modify the photocatalytic activity [23,24]. The energy band positions and a proposed scheme for the photooxidation mechanism under irradiation are presented in Fig. 5. Because of the potential difference in the conduction and valence band of the components, the photogenerated electrons on the Conduction Band of Cu_2O will transfer to CuO, then to TiO_2. The proposed photo redox results electron-hole pair separation leading to lower recombination [25]. Furthermore, the selectivity factor for reaction products extracted from the data was presented in Table.2. The selectivity is a dimensionless parameter runs for all products of the photodegradation reaction. In this work, Acetone (Ac) and carbon dioxide (CO_2) are two main compounds obtained as 2-propanol photodegradation reaction products for all samples, in agreements with reported studies [26,27].

Finally, the stability of the samples reacted under UV and sunlight-type illumination conditions by the XRD analysis of the samples are shown in Fig. 6 and compared to the fresh samples (Fig. 1). No significant differences are observed between fresh and used materials. The results revealed that the samples prepared in this research are stable and can be used as promising materials for photocatalytic performance. In agreement with litrature, the copper species instability problem could be modified by using a mixture of CuO and Cu_2O [6]. Furthermore, TiO_2 is a chemical stable photocatalyst and formation the heterostructure with copper species could promote the stability of the samples [28].

4. Conclusions

The CuO-Cu_2O/TiO_2 nanocomposite materials were successfully synthesized by using two step including solution treatment and sol-gel method and further characterized with various techniques. The gas-phase photo-oxidation of 2-propanol under UV and sunlight type illumination was used to evaluate the photocatalytic performance

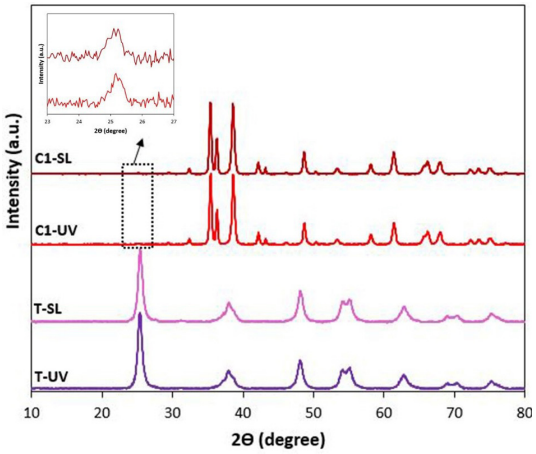

Fig. 6- XRD patterns of the samples after photocatalytic reactions under UV and Sunlight type illumination.

of the samples prepared by the sol-gel method in this study. Obtained results demonstrated that these nanocomposites provide enhanced photocatalytic performance compared to the TiO_2 reference because of successful formation of heterostructure with desirable structure and morphology. Moreover, the important role of the calcination process factors was evaluated on the properties and photocatalytic activity. The high activity obtained for the nanocomposite sample for both UV and sunlight illumination conditions might be due to the co-existence of the Cu species (CuO, Cu_2O) in the structure and TiO_2 phase on the surface. Furthermore, it is proved that these nanocomposites are stable for photoactivity applications.

5. Acknowledgement

The authors would like to acknowledge the support of the University of Tehran and the Iran Nanotechnology Initiative Council for this research. CSIC is acknowledged for supporting experiments carried out at ICP.

References

1. Palmisano G, García-López E, Marcì G, Loddo V, Yurdakal S, Augugliaro V, et al. Advances in selective conversions by heterogeneous photocatalysis. Chemical Communications. 2010;46(38):7074.
2. Ajmal A, Majeed I, Malik RN, Iqbal M, Nadeem MA, Hussain I, et al. Photocatalytic degradation of textile dyes on Cu2O-CuO/TiO2 anatase powders. Journal of Environmental Chemical Engineering. 2016;4(2):2138-46.
3. Deng X, Wang C, Shao M, Xu X, Huang J. Low-temperature solution synthesis of CuO/Cu2O nanostructures for enhanced photocatalytic activity with added H2O2: synergistic effect and mechanism insight. RSC Advances. 2017;7(8):4329-38.
4. Valles-Pérez BY, Badillo-Ávila MA, Torres-Delgado G, Castanedo-Pérez R, Zelaya-Ángel O. Photocatalytic activity of ZnO + CuO thin films deposited by dip coating: coupling effect between oxides. Journal of Sol-Gel Science and Technology. 2020;93(3):517-26.
5. Scuderi V, Amiard G, Boninelli S, Scalese S, Miritello M, Sberna PM, et al. Photocatalytic activity of CuO and Cu2O nanowires. Materials Science in Semiconductor Processing. 2016;42:89-93.
6. Chen J, Liu X, Zhang H, Liu P, Li G, An T, et al. Soft-template assisted synthesis of mesoporous CuO/Cu 2 O composite hollow microspheres as efficient visible-light photocatalyst. Materials Letters. 2016;182:47-51.
7. Kubacka A, Muñoz-Batista MJ, Fernández-García M, Obregón S, Colón G. Evolution of H2 photoproduction with Cu content on CuO -TiO2 composite catalysts prepared by a microemulsion method. Applied Catalysis B: Environmental. 2015;163:214-22.
8. Liu L, Yang W, Li Q, Gao S, Shang JK. Synthesis of Cu2O Nanospheres Decorated with TiO2 Nanoislands, Their Enhanced Photoactivity and Stability under Visible Light Illumination, and Their Post-illumination Catalytic Memory. ACS Applied Materials & Interfaces. 2014;6(8):5629-39.
9 Ren H, Koshy P, Chen W-F, Qi S, Sorrell CC. Photocatalytic materials and technologies for air purification. Journal of Hazardous Materials. 2017;325:340-66.
10. Nuo Peh CK, Wang X-Q, Ho GW. Increased photocatalytic activity of CuO/TiO 2 through broadband solar absorption heating under natural sunlight. Procedia Engineering. 2017;215:171-9.
11. Kim HR, Razzaq A, Grimes CA, In S-I. Heterojunction p-n-p Cu 2 O/S-TiO 2 /CuO: Synthesis and application to photocatalytic conversion of CO 2 to methane. Journal of CO2 Utilization. 2017;20:91-6.
12. Luna AL, Valenzuela MA, Colbeau-Justin C, Vázquez P, Rodriguez JL, Avendaño JR, et al. Photocatalytic degradation of gallic acid over CuO–TiO2 composites under UV/Vis LEDs irradiation. Applied Catalysis A: General. 2016;521:140-8.
13. Tian X, Li S, Cao Y, Xu Y, Zhang G. Preparation, optical property, and photocatalytic activity of cubic Cu2O/amorphous TiO2 and spheric CuO/TiO2 core–shell nanocomposites. Materials Letters. 2014;131:86-9.
14. Muñoz-Batista MJ, Caudillo-Flores U, Ung-Medina F, del Carmen Chávez-Parga M, Cortés JA, Kubacka A, et al. Gas phase 2-propanol degradation using titania photocatalysts: Study of the quantum efficiency. Applied Catalysis B: Environmental. 2017;201:400-10.
15. Mamba G, Pulgarin C, Kiwi J, Bensimon M, Rtimi S. Synchronic coupling of Cu2O(p)/CuO(n) semiconductors leading to Norfloxacin degradation under visible light: Kinetics, mechanism and film surface properties. Journal of Catalysis. 2017;353:133-40.
16. Murali DS, Kumar S, Choudhary RJ, Wadikar AD, Jain MK, Subrahmanyam A. Synthesis of Cu2O from CuO thin films: Optical and electrical properties. AIP Advances. 2015;5(4):047143.
17. Rouquerol J, Avnir D, Fairbridge CW, Everett DH, Haynes JM, Pernicone N, et al. Recommendations for the characterization of porous solids (Technical Report). Pure and Applied Chemistry. 1994;66(8):1739-58.
18. Xu L, Xu H-Y, Wang F, Zhang F-J, Meng Z-D, Zhao W, et al. Microwave-Assisted Synthesis of Flower-like and Plate-like CuO Nanopowder and Their Photocatalytic Activity for Polluted Lake Water. Journal of the Korean Ceramic Society. 2012;49(2):151-4.

19. Ansari F, Sheibani S, Fernández-García M. Characterization and performance of Cu2O nanostructures on Cu wire photocatalyst synthesized in-situ by chemical and thermal oxidation. Journal of Materials Science: Materials in Electronics. 2019;30(14):13675-89.
20. Shafei A, Sheibani S. Visible light photocatalytic activity of Cu doped TiO2-CNT nanocomposite powder prepared by sol–gel method. Materials Research Bulletin. 2019;110:198-206.
21. Hu Z, Wang X, Dong H, Li S, Li X, Li L. Efficient photocatalytic degradation of tetrabromodiphenyl ethers and simultaneous hydrogen production by TiO2-Cu2O composite films in N2 atmosphere: Influencing factors, kinetics and mechanism. Journal of Hazardous Materials. 2017;340:1-15.
22. Khaki MRD, Shafeeyan MS, Raman AAA, Daud WMAW. Application of doped photocatalysts for organic pollutant degradation - A review. Journal of Environmental Management. 2017;198:78-94.
23. Wang P, Wen X, Amal R, Ng YH. Introducing a protective interlayer of TiO2 in Cu2O–CuO heterojunction thin film as a highly stable visible light photocathode. RSC Advances. 2015;5(7):5231-6.
24. Dasineh Khiavi N, Katal R, Kholghi Eshkalak S, Masudy-Panah S, Ramakrishna S, Jiangyong H. Visible Light Driven Heterojunction Photocatalyst of CuO–Cu2O Thin Films for Photocatalytic Degradation of Organic Pollutants. Nanomaterials. 2019;9(7):1011.
25. Lu Y, Zhang X, Chu Y, Yu H, Huo M, Qu J, et al. Cu2O nanocrystals/TiO2 microspheres film on a rotating disk containing long-afterglow phosphor for enhanced round-the-clock photocatalysis. Applied Catalysis B: Environmental. 2018;224:239-48.
26. Muñoz-Batista MJ, Kubacka A, Hungría AB, Fernández-García M. Heterogeneous photocatalysis: Light-matter interaction and chemical effects in quantum efficiency calculations. Journal of Catalysis. 2015;330:154-66.
27. Araña J, Alonso AP, Rodríguez JMD, Colón G, Navío JA, Peña JP. FTIR study of photocatalytic degradation of 2-propanol in gas phase with different TiO2 catalysts. Applied Catalysis B: Environmental. 2009;89(1-2):204-13.
28. Xiong D, Chang H, Zhang Q, Tian S, Liu B, Zhao X. Preparation and characterization of CuCrO2/TiO2 heterostructure photocatalyst with enhanced photocatalytic activity. Applied Surface Science. 2015;347:747-54.